
Proceedings Paper:
Wang, Yi, MARVIN, ANDY, BALE, SIMON JONATHAN et al. (2026) Investigation of the feasibility of near-field magnetic shielding measurements in the 10 MHz to 200 MHz frequency range. In: International Symposium on Electromagnetic Compatibility - EMC Europe 2026. IEEE International Symposium on Electromagnetic Compatibility. IEEE. (In Press)

Investigation of the feasibility of near-field magnetic shielding measurements in the 10 MHz to 200 MHz frequency range

Yi Wang
School of Physics Engineering and Technology
University of York
York, UK
yi.wang2@york.ac.uk

Andrew C Marvin
School of Physics Engineering and Technology
University of York
York, UK
andy.marvin@york.ac.uk

Simon J Bale
School of Physics Engineering and Technology
University of York
York, UK
simon.bale@york.ac.uk

Ali Ghaffarlouy Raef
School of Physics Engineering and Technology
University of York
York, UK
ali.raef@york.ac.uk

John Dawson
School of Physics Engineering and Technology
University of York
York, UK
john.dawson@york.ac.uk

Martin Robinson
School of Physics Engineering and Technology
University of York
York, UK
martin.robinson@york.ac.uk

***Abstract*—The use of electrostatically shielded loops for the near-field measurement of Shielding Effectiveness (SE) of planar conducting materials at frequencies above those covered by current standards is examined by simulation and measurement. The transverse wave impedances of the shielded loops are shown to be dependent on the loop orientation as are resulting measured shielding effectiveness values.**

Keywords—magnetic field shielding effectiveness, simulation, measurements

I. INTRODUCTION

Power electronic converters are used in a wide range of applications, including transportation systems, renewable energy systems and consumer electronics. To increase efficiency and power density, many systems employ high-speed semiconductor switching devices, producing switching transients whose waveforms are rich in harmonics extending to frequencies of 100 MHz or more [1]. The magnetic fields generated by these systems require shielding. Structures around these systems may be made from composite materials and the magnetic near-field shielding performance of these materials requires evaluation.

The use of electrostatically shielded loop antennas for the measurement of near-field magnetic shielding effectiveness (SE) is well established. For example, in IEEE Std 299 [2] and NSA 94-106 [3] such loops are used for evaluating the SE of enclosures at frequencies up to 20 MHz. At frequencies above 20 MHz biconical dipole antennas are used. In this paper we examine the feasibility of using electrostatically shielded loops for the measurement of the SE of conducting materials in the frequency range up to 200 MHz. Conventional shielded loops have diameters of 300 mm or more. Here we use smaller loops initially with a loop diameter of 100 mm. There have been many studies of the measurement of magnetic near-field shielding.

The examples in [4] and more recently [5] are mostly based on the well-known Schelkunoff theory of plane wave SE which splits the SE of an infinite sheet of material into reflection, absorption and multiple transit contributions [6]. The Schelkunoff theory is modified to account for the transverse wave impedance of the loop antennas differing from that of free space. In [4] a theoretical approach is taken with no measured results being presented. In both [5] and [7] simulation studies are undertaken, illustrating the importance of the transverse wave impedance of the loops. Measured data are included in [7]. There are two viable orientations of a pair of loops, coplanar and coaxial, as shown in Fig. 1. The work in [5] illustrates the differences between a pair of coplanar loops as used in [2] and a pair of coaxial loops as used in [3].

Here we use the coplanar loop orientation with electrostatically shielded loops. No previous work has been found that examines the details of the transverse wave impedance of either shielded or unshielded loops accounting for the asymmetries introduced into the loop by the feed point internal impedance and, in the case of a shielded loop, the gap in the electrostatic shield. These structural properties of a loop, present in any physical loop implementation, are shown to significantly modify the transverse wave impedance of the near-field generated by the loops and to have a significant influence on the measured SE of a sheet of conducting material.

In Section II the calculated and simulated transverse wave impedances of the fields generated by unshielded and shielded loops are presented illustrating the effect of the position of the observation point on the transverse wave impedance values. In Section III the measurement techniques and measured values of the transverse wave impedance of a

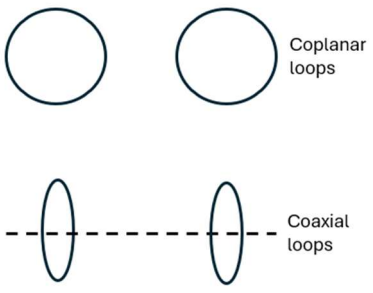

Fig. 1. Coplanar and coaxial loop orientations.

This project has received funding from the European Union's EU Framework Program for Research and Innovation Europe Horizon (Grant Agreement No 101072881) and UKRI (EP/X033481/1).

100 mm diameter shielded loop are presented confirming the predictions presented in Section II. Section IV describes the simulation and measurement of the SE of a sheet of planar material illustrating the effects of loop position and orientation on the simulated and measured results. Conclusions are drawn in Section V.

II. Transverse Wave Impedance Simulations of Fields Radiated from Loops

A. Unshielded Loops

The fields radiated by an electrically small circular loop (a magnetic dipole) in free space are well known and are given by the equations below [8]. Consider a circular loop of radius a centred at the origin of the spherical co-ordinate system (r, θ, ϕ) with the loop lying in the ϕ plane defined by $\theta = \pi/2$. The loop carries a current I at angular frequency ω. In the plane of the loop, $\theta = \pi/2$, two field components are present, the electric field E_ϕ and the magnetic field H_θ. The radial magnetic field component H_r is zero in this case.

$$E_\phi = -\frac{j\omega\mu I a^2}{4}\left(\frac{j\omega\sqrt{\mu\epsilon}}{r}+\frac{1}{r^2}\right)e^{-j\omega\sqrt{\mu\epsilon}r}\sin(\theta) \quad (1)$$

$$H_\theta = \frac{j\omega\mu I a^2}{4}\left(\frac{j\omega\varepsilon}{r}+\frac{1}{j\omega\mu r^3}+\frac{1}{\sqrt{\frac{\mu}{\varepsilon}}r^2}\right)e^{-j\omega\sqrt{\mu\varepsilon}r}\sin(\theta) \quad (2)$$

Here μ and ε are the magnetic permeability and electric permittivity of free space. In the reactive near-field the transverse wave impedance is defined in (3) as Z_T.

$$Z_T = \frac{E_\phi}{H_\theta} \quad (3)$$

Fig. 2 shows the magnitude of the transverse wave impedance, calculated from (1) and (2), for a loop of 50 mm radius in the frequency range up to 200 MHz at different distances from the loop centre in the $\theta = \pi/2$ plane.

The calculated wave impedances show the characteristic rising wave impedance with frequency that peaks and then becomes asymptotic to 377 Ω, the intrinsic impedance of free space. The associated phase of the transverse wave impedance is shown in Fig. 3. The phase shows the expected characteristic transition from an inductive impedance to a real impedance as the frequency increases.

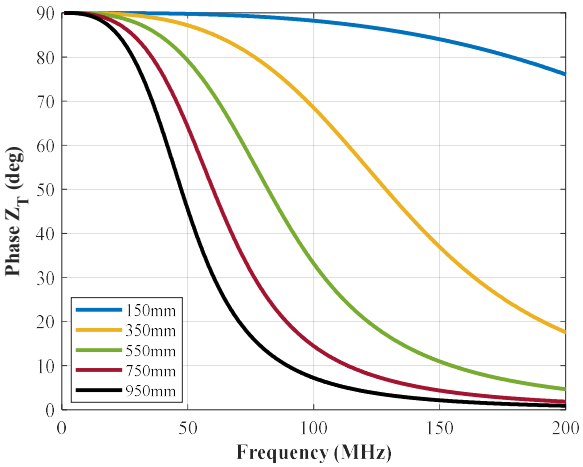

Fig. 3. Phase of the transverse wave impedance of a 50 mm radius loop at distances between 150 mm and 950 mm from the loop centre.

In practice, such a loop cannot be realised as there is no drive point. The frequency domain solver in CST Microwave Studio ™ was used to simulate a 50 mm radius loop of 1 mm diameter wire. The loop was driven from an excitation port with 50 Ω internal impedance representing an idealised practical scenario. The drive point is at $\phi = 180$ degrees.

Fig. 4 shows the simulated magnitude of the transverse wave impedance. The distance from the loop centre is along a line out from the loop opposite to the excitation port ($\phi = 0$ degrees direction). Fig. 5 shows simulated wave impedance magnitudes for the case where the distances are along a line at right angles to those of Fig. 4, i.e. $\phi = 90$ degrees.

Comparison of Figs 2, 4, and 5 shows that whilst the overall trend is maintained, the introduction of a drive point into the loop with a finite internal impedance removes the symmetry of the loop in the ϕ direction. This causes alterations in the wave impedance magnitudes and also introduces a directional dependency with the transverse wave impedance generally being lower at distances in a direction opposite the feed point at $\phi = 0$ degrees compared to $\phi = 90$ degrees.

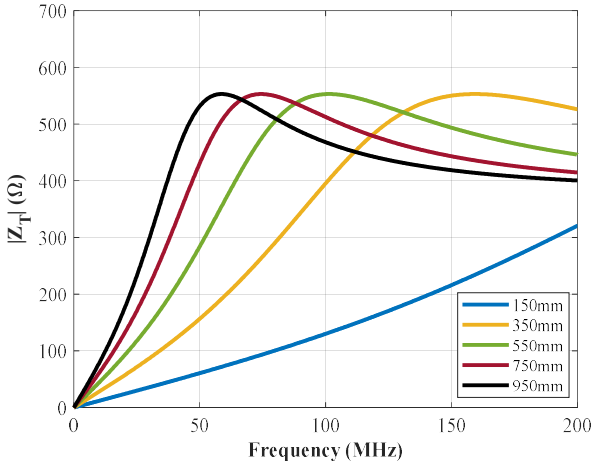

Fig. 2. Calculated magnitude of the transverse wave impedance of a 50 mm radius loop at distances between 150 mm and 950 mm from the loop centre.

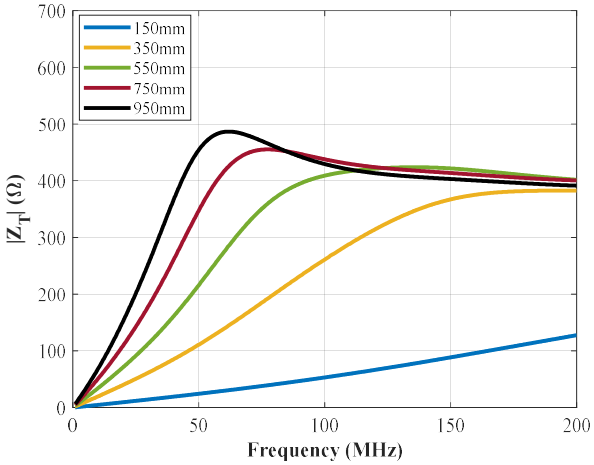

Fig. 4. Simulated magnitude of the transverse wave impedance of a 50 mm radius loop at distances between 150 mm and 950 mm from the loop centre ($\phi = 0$ degrees).

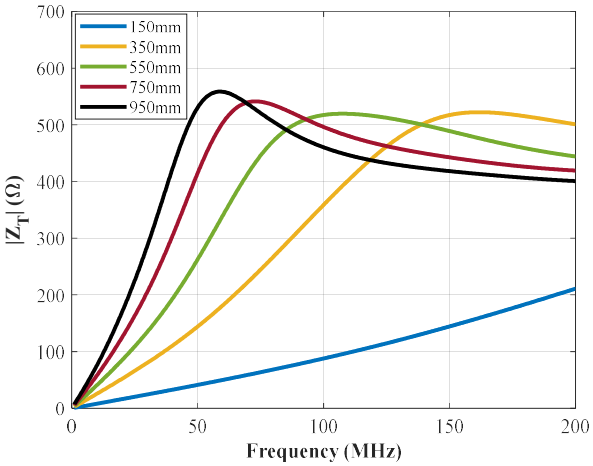

Fig. 5. Simulated magnitude of the transverse wave impedance of a 50 mm radius loop at distances between 150 mm and 950 mm from the loop centre ($\phi = 90$ degrees).

B. *Shielded Loops*

Shielded loops are more commonly used in near-field magnetic field measurements where the shield is intended to reduce the loop's response to local electric fields. However, the fields generated by shielded loops are also of importance where pairs of loops are used for SE measurements.

Fig. 6 shows a representation of a 50 mm radius shielded loop with the loop shield and internal conductor formed from RG402 semi-rigid coaxial cable. The inner conductor radius is 0.46 mm, the dielectric radius is 1.49 mm and the outer conductor radius is 1.79 mm. The shield is broken by a 10 mm long gap at the left side of the diagram. The balanced feed is formed by the extended coaxial cables on the right of the diagram the outer conductors of which are connected together. These form a 100 Ω characteristic impedance balanced transmission line. The loop is driven by two 50 Ω internal impedance sources connected, in anti-phase, between the inner and outer conductors to give an overall 100 Ω internal

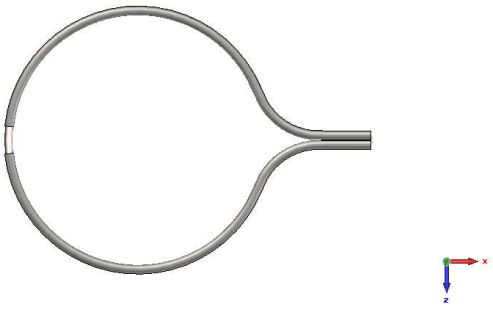

Fig. 6. CST representation of a shielded loop of 50 mm radius formed from RG402 coaxial cable. The curved sections between the loop and the balanced feed have a 25 mm radius.

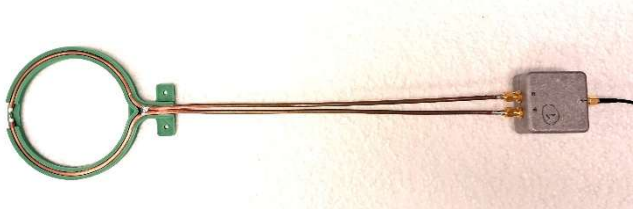

Fig. 7. Shielded loop, 100 mm diameter, made from RG402, on a 3D printed plastic former. The balanced feed transmission line is fed from a 2:1 impedance ratio balun transformer in the diecast box to the right.

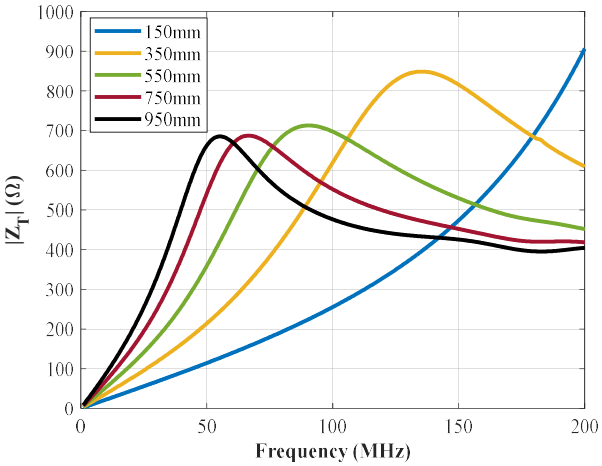

Fig. 8. Simulated transverse wave impedance magnitudes for the shielded loop depicted in Fig. 6 in the $\phi = 0$ degree direction.

impedance balanced source. Fig. 7 is an image of the loop as realised.

This structure (Fig. 6) was simulated using the CST frequency domain solver. Fig. 8 shows the resulting wave impedance magnitude data for distances from the loop in the $\phi = 0$ degrees direction which crosses the shield gap. Fig. 9 shows comparable data for distances from the loop centre extending in the $\phi = 90$ degrees direction.

The data show significant differences between the two directions with transverse wave impedances in the direction opposite to the shield gap being significantly larger than those in the orthogonal direction. These results indicate a significant relative increase in the electric field in the direction out from the loop centre crossing the shield gap ($\phi = 0$ degrees) compared to the orthogonal direction ($\phi = 90$ degrees).

III. Transverse Wave Impedance Measurements

In this section measurements of the transverse wave impedance of a 50 mm radius shielded loop are described. The magnetic fields generated by the shielded loop were measured using a balanced shielded loop field probe and the electric fields were measured using a balanced electric dipole field probe. Each was connected in turn to a broadband balun. Fig. 10 shows an image of the two probes and the balun.

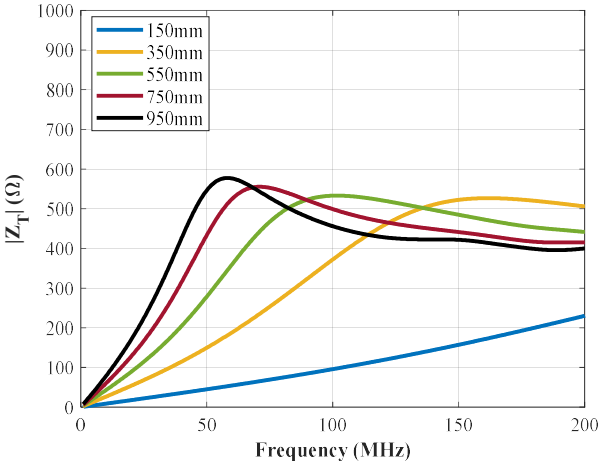

Fig. 9. Simulated transverse wave impedance magnitudes for the shielded loop depicted in Fig. 6 in the $\phi = 90$ degree direction.

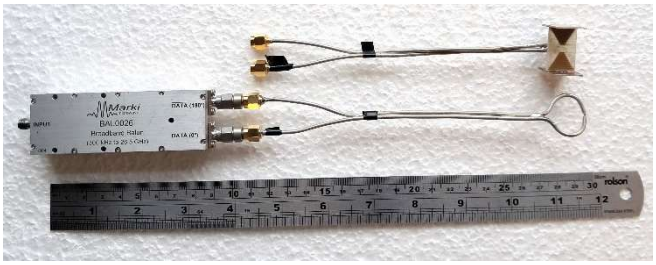

Fig. 10. Image of the electric dipole field probe and the shielded magnetic loop field probe and the balun.

A. Electric and Magnetic field probe calibration.

In order to measure the transverse wave impedance the electric and magnetic field probes required calibration. A 50 Ω characteristic impedance parallel plate transmission line as shown in Fig. 11 was used.

The ratio of electric to magnetic field between the transmission line plates is 377 Ω. Using a Vector Network Analyser (VNA), the complex forward scattering parameter between the parallel plate transmission line input and the field probe output was measured for electric and magnetic field probes, $S21E_{cal}$ and $S21H_{cal}$ respectively. Similar complex forward scattering parameter measurements using a VNA are made between the input port of the shielded loop and the electric and magnetic field probe output, $S21E_{loop}$ and $S21H_{loop}$ respectively. The measured loop transverse wave impedance is thus Z_T:

$$Z_T = \frac{S21E_{loop}}{S21H_{loop}} . \frac{S21H_{cal}}{S21E_{cal}} . 377 \qquad (4)$$

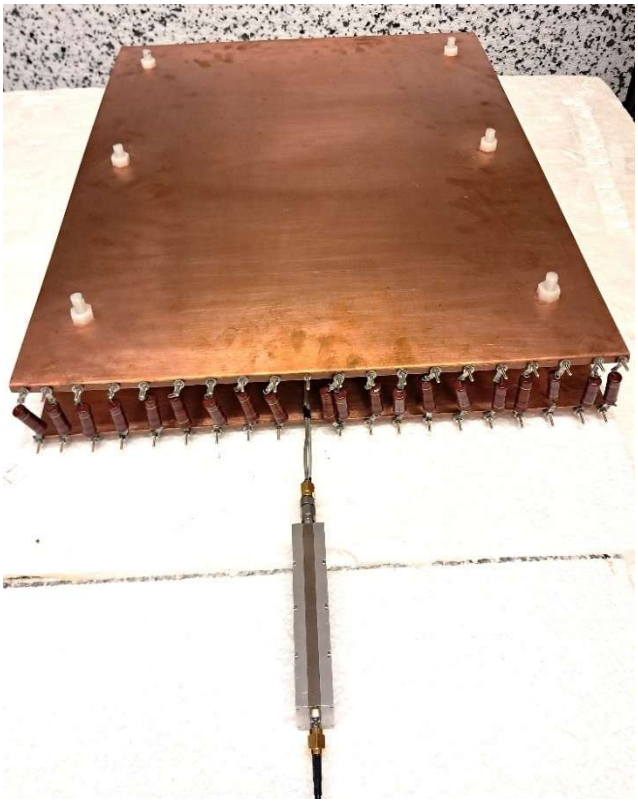

Fig. 11. The parallel plate transmission line showing the distributed matched load resistors and the field probe inserted between the plates. The parallel plate transmission line feed point is at the top of the image. The field probe balun remains outside the transmission line.

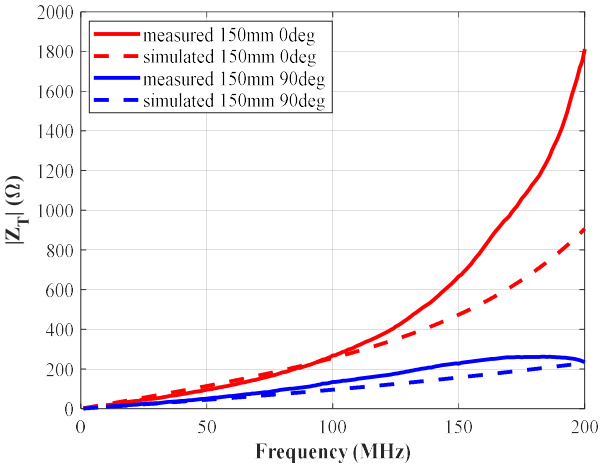

Fig. 12. Measured and simulated transverse wave impedance of the 50 mm radius shielded loop at a distance of 150 mm from the loop centre. The solid line is measured, and the dotted line is simulated.

B. Measured Transverse Wave Impedance Results

Examples of the measured and simulated transverse wave impedances are shown in Fig. 12 and Fig. 13. Whilst the simulations and measurements show some differences, particularly above 100 MHz, the trend of the results is clear. The measurements demonstrate that the transverse wave impedance in the near-field of the shielded loop depends on both distance and direction from the loop centre in the manner indicated by the simulations. The measurement frequency range is 10 MHz to 200 MHz and no anechoic chamber covering this frequency range was available. The measurements were performed in the open laboratory as far as possible from other objects. However, they were sensitive to their immediate surroundings particularly as the separation from the shielded loop centre increased and the field strength reduced. For this reason measurements at distances greater than 350 mm are not included.

IV. Simulation and Measurement of Magnetic Near-Field Shielding Effectiveness

The data shown in Sections II and III above show that the near-field transverse wave impedance of a shielded loop

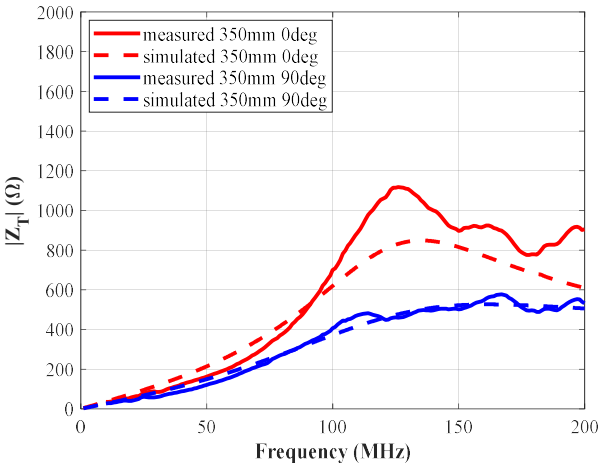

Fig. 13. Measured and simulated transverse wave impedance of the 50 mm radius shielded loop at a distance of 350 mm from the loop centre. The solid line is measured, and the dotted line is simulated.

depends on the orientation of the measurement direction in the plane of the loop. In this section the effect of the changed wave impedance on the measurement of the SE of a planar conducting sheet is investigated.

Two 50 mm radius shielded loops were used in simulation and measurement of the magnetic near-field SE of a planar sheet of conductive material. The material used is a non-woven veil made from 6 mm long 7 µm diameter carbon fibres using a wet-laying process. The material is 300 µm thick. Our four-point probe resistivity measurement gave a material conductivity of 670 S/m comparable to the figure in the material data sheet (34 g/m^2 Optiveil 20301A® by Technical Fibre Products Ltd).

Two strips of the 600 mm wide veil was sandwiched between two polystyrene sheets to form a 1.2 m square sheet. Images of the measurement set-up are shown in Fig. 14.

In the images of Fig. 14 the shielded loop shield gap is closest to the veil corresponding to the zero degree loop orientation.

The SE was measured by taking the ratio of the coupling between the two loops (S_{21} measured using a VNA) with and without the veil present. The CST time domain solver was used to simulate the measurement with the 1.2 m square veil

Fig. 14. Images of the SE measurement set-up for a loop to shield distance of 150 mm. The shield material veil is sandwiched between two polystyrene sheets.

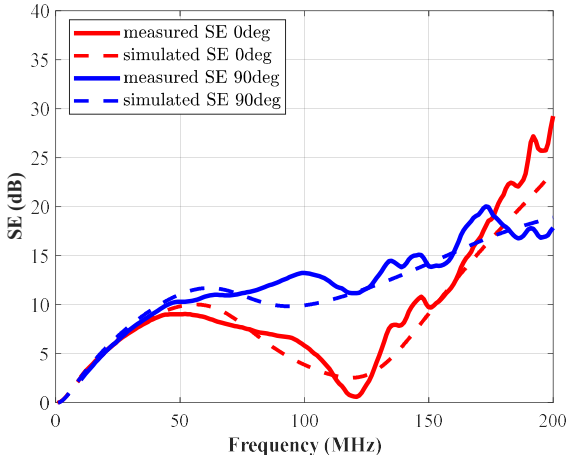

Fig. 15. Simulated and measured SE of the 1.2 m square veil for two orientations of the shielded loops. Angles in the key refer to the orientation of the loops. Each loop is 150 mm from the veil.

and also with an infinite veil. Fig. 15 shows the measured and simulated results for the 1.2 m square veil with the shielded loops placed 150 mm from the veil. The zero degree results are for where the shield gaps are initially closest to the veil; the 90 degrees results are for the loops rotated by 90 degrees from that initial position (see Fig. 14).

The measured and simulated results are in acceptable agreement with deviations in the measured results attributed to the non-ideal measurement surroundings. It can be seen that the loop orientation associated with higher transverse wave impedance (0 degrees) results in a generally lower SE.

Fig. 16 shows the comparison between the simulated SE of the veil for a 1.2 m square veil and an "infinite" veil (veil extends to computational boundary). For the "infinite" veil simulation, 50 mm radius shielded loops were placed 150 mm from the veil on either side. These results demonstrate the effect of a finite veil sample size on the measurement of SE.

As would be expected, the infinite veil SE is larger than the finite veil SE with the difference becoming more marked as the frequency increases. The reduction in simulated SE for the 1.2 m veil is attributed to leakage around the finite sample edge. The overall trend of the SE variation with increasing frequency is the same in both cases.

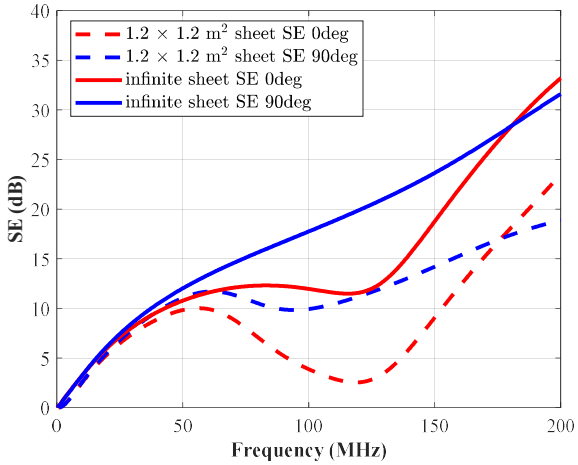

Fig. 16. Comparison of the simulated SE values for an infinite veil and a 1.2 m square veil. Angles in the key refer to the orientation of the loops. Each loop is 150 mm from the veil.

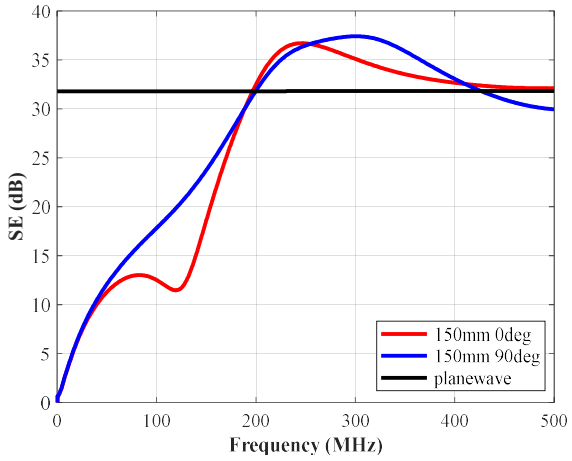

Fig. 17. Comparison between the simulated SE values for an infinite veil with 50 mm radius shielded loops 150 mm from the veil and the simulated Schelkunoff plane wave SE over an extended frequency range to 500 MHz.

It is emphasised that the simulated data for the infinite veil are not the same as standard Schelkunoff plane wave SE data. Fig. 17 shows the comparison between the simulated infinite veil SE for both shielded loop orientations and the simulated plane wave SE as proposed by Schelkunoff [6] over an extended frequency range to 500 MHz. At 500 MHz the 150 mm loop to veil separation is a quarter wavelength and the transverse wave impedance of the loops is converging to 377 Ω at this separation distance. The simulated SE values also converge.

V. Conclusions

In this paper the feasibility of measuring the magnetic near-field SE of conducting materials in the frequency range up to 200 MHz has been investigated. Measured and simulated results are in acceptable agreement. The results in both simulation and in measurement demonstrate the importance of the orientation of the loops used in the measurement reflecting the dependence of the loop transverse wave impedance on the loop orientation with respect to the shielded loop shield gap and the loop feed point. Simulations and measurements of the transverse wave impedance of electrostatically shielded loops have demonstrated significant differences in transverse wave impedance between shielded loops and unshielded loops which are critical to the eventual measured values of SE.

The results presented here demonstrate that, as with any SE measurement technique, Schelkunoff included, the interpretation and application of the results requires care as the results depend not only on the material under test but also on the measurement system itself.

References

[1] B. Zhang and S. Wang, “A survey of EMI research in power electronics systems with wide-bandgap semiconductor devices,” IEEE J. Emerg. Sel. Top. Power Electron., vol. 8, no. 1, pp. 626–643, Mar. 2020

[2] "IEEE Standard Method for Measuring the Effectiveness of Electromagnetic Shielding Enclosures," in IEEE Std 299-2006 (Revision of IEEE Std 299-1997) , vol., no., pp.1-52, 28 Feb. 2007, doi: 10.1109/IEEESTD.2007.323387.

[3] NSA 94–106: Specification for shielded enclosures, National Security Agency, Fort George G. Meade, MD, USA, Tech. Rep. 24, 1994.

[4] J. Ronald Moser “Low-Frequency Shielding of a Circular Loop Electromagnetic Field Source” in IEEE Transactions on Electromagnetic Compatibility, vol 9, no 1, pp 6-18, March 1967.

[5] L. Koraqi, T. Claeys, J. Catrysse and D. Pissoort, "Differences Between NSA 94–106 and IEEE Std. 299 Setups for Low-Frequency Magnetic Shielding Effectiveness Characterization: A Study Using Numerical Simulations," in IEEE Letters on Electromagnetic Compatibility Practice and Applications, vol. 6, no. 1, pp. 22-28, March 2024, doi: 10.1109/LEMCPA.2024.3355849.

[6] S. A. Schelkunoff. “Electromagnetic Waves”. D. van Nostrand Company Inc., 1943, pp. 303–312

[7] L. Koraqi et al., "Low-Frequency Magnetic Shielding Effectiveness Characterization of Planar Materials: Measurements and Numerical Simulations," in IEEE Transactions on Electromagnetic Compatibility, vol. 67, no. 5, pp. 1450-1461, Oct. 2025, doi: 10.1109/TEMC.2025.3574758.

[8] S. Ramo, J. R. Whinnery and T Van Duzer, “Fields and Waves in Communication Electronics” John Wiley and Sons, 1994.